IEEE Access
Multidisciplinary | Rapid Review | Open Access Journal

Received July 3, 2019, accepted August 2, 2019, date of publication August 16, 2019, date of current version August 29, 2019.

Digital Object Identifier 10.1109/ACCESS.2019.2935815

Depth Control for a Deep-Sea Self-Holding Intelligent Buoy Under Ocean Current Disturbances Based on Finite-Time Boundedness Method

ZURONG QIU[1], QIANG WANG[1,2], HONGYU LI[2,3], SHAOBO YANG[1,2], AND XINGFEI LI[1,2]

[1]State Key Laboratory of Precision Measuring Technology and Instruments, Tianjin University, Tianjin 300072, China
[2]Qingdao Institute for Ocean Technology, Tianjin University, Qingdao 266200, China
[3]School of Mechanical and Electronic Engineer, Shandong University of Science and Technology, Qingdao 266590, China

Corresponding author: Xingfei Li (lixftju@sohu.com)

This work was supported in part by the Wenhai Program of the Qingdao National Laboratory for Marine Science and Technology under Grant 2017WHZZB0101, and in part by the Demonstration Project of Marine Economic Innovation and Development for the National 13th Five-Year Plan under Grant BHSF2017-27.

ABSTRACT In order to achieve the rejection of the ocean current disturbances and fast convergence in the depth positioning process of the deep-sea self-holding intelligent buoy (DSIB), a finite-time boundedness (FTB) depth control strategy based on over shoot estimation in pole placements (OEIPP) method has been proposed in which variable gains are adjusted for the DSIB closed-loop system. In this paper, the system parameters have been investigated including depth error, transient time, control gains and current disturbances. The mathematical model for the DSIB dynamic motion is established by combining the pressure hull deformation and the current disturbances model. At the same time, as the DSIB closed-loop system need be established by the finite-time transformation matrix, the establishment process on the FTB depth control strategy with a OEIPP method has been proofed. Finally, to observe the transient state of the DSIB closed-loop control system in finite time, an adjustment rule of the control gains under different current disturbances based on the FTB depth control method is analyzed. The performance of the control strategy is validated through simulations and at-sea experiments, and its feasibility established. The results show that the proposed control strategy can guarantee that the DSIB reaches the allowable depth errors of a target depth under the ocean current disturbances within a finite time. They also provide a useful guide for establishing an adjustment rule for the control gains under various current disturbances within a finite time.

INDEX TERMS Deep-sea self-holding intelligent buoy (DSIB), finite-time boundedness (FTB), depth control, overshoot estimation in pole placements (OEIPP), ocean current disturbances.

I. INTRODUCTION

A DSIB (deep-sea self-holding intelligent buoy), which is also known as a profiling float or a Lagrangian float, dives, and ascends by changing its buoyancy [1], [2]. Marine data such as profiles of temperature, salinity, and depth with vertical cycles can be measured by this device. These data are transmitted to the ground through satellites, as shown in Fig. 1. The DSIB is widely used to provide information for ocean development and research, weather forecasting. and naval and military activities [1]–[4]. Recent observation-based studies demonstrated that the warming of the deep oceans below 2000 m has significantly contributed to the mean sea level rise [12]. Hence, it is necessary to obtain a deeper observation data for expanding the DSIB coverage into the deep ocean below 2000 m. To achieve this objective, a control method for depth positioning of the DSIB is indispensable. Depth positioning is an important function of a DSIB. However, the dynamics of the DSIB have nonlinear relation with the environmental disturbances. Several control methods for nonlinear depth positioning have been proposed, which, however, render the depth positioning

The associate editor coordinating the review of this article and approving it for publication was Nasim Ullah.

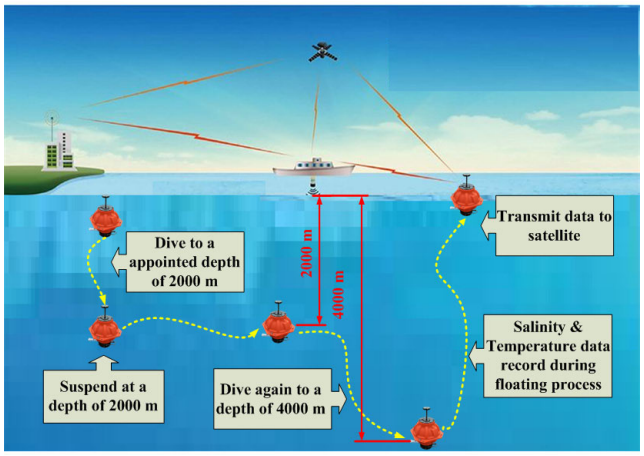

FIGURE 1. Observation scheme of DSIB.

method difficult to design [15], [16]. Many researchers have extensively investigated various linear control approaches as well, and their achievements have been acknowledged in the current literature [7], [8], [13], [15], [16], [23].

For the DSIB, following methods are used to design the depth positioning controller. One such earlier depth positioning method is the proportional-integral-derivative (PID) feedback law [7], [13], which was successfully used in practice. The PID controller [7] was utilized to control the depth and altitude above the bottom of the ocean. Although this PID controller was effective, it was difficult to optimize the control parameters in the depth control process. Similarly, a discrete PID controller with a second-order low-pass filter was used in depth positioning. However, the convergence time of system need be improved in the foregoing method [13]. Other studies available in literature [8], [23] are related to the state–space feedback control algorithm. The control algorithm proposed in [8] was used not only to increase the accuracy of the float dynamics model, but also to accomplish the control procedure for depth positioning and altitude trajectory. However, this method had to be combined with empirical motor efficiency data so that the tradeoffs between the efficiency and the control performance could be studied. On the other hand, DSIB in practice must also be capable of operating in the depth positioning process subject to ocean currents. However, few results on the ocean current disturbances can't be found in the above works [7], [8], [13]. In order to compensate the influence of the currents, a simple feedback method called steady-state depth errors response controller [23] was recommended for depth positioning under current disturbances, but the complete applicability of this control method was not authenticated. Another intelligent control strategy based on the ocean model was used to design the depth positioning strategy [15], [16]. Their ocean model predictions were applied to facilitate a basic level of autonomy [15]. In [16], an ocean-scale sensor web was recommended on the basis of intelligent depth positioning. Nevertheless, the two algorithms presented in [15], [16] were dependent on a large-scale ocean model.

Although the control algorithms mentioned above [7], [8], [13], [15], [16], [23] have shown adequate reliability in DSIB depth positioning, the aforementioned control methods only guaranteed asymptotical stability and performance criteria defined over an infinite time from different depth control perspectives. Before a DSIB can be deployed, the control parameters and the finite control time need to be determined; however, the external current disturbances may lead to unavoidable disturbances in the depth control process. Moreover, the depth control system considerably depends on the accuracy of the hydrodynamic model of the DSIB. The external current disturbances tend to increase the complexities and difficulties in the float's model, and can render the float uncontrollable at a target depth during the finite control time. Therefore, analyzing the transient state of the depth control system precisely during the finite control time is necessary. Compared with infinite-time depth control methods presented in [7], [8], [13], [15], [16], [23], the closed-loop system under the finite-time control law possesses strong anti-jamming features and a fast convergence rate. Hence, this control law has attracted the attention of a growing number of researchers [14], [17]–[20], [25], [26].

Some early results based on the concept of finite-time control law dated back to the 1960s, [17], [18], wherein, the concept of FTS (finite time stability) was introduced. To deal with the coordination control problem of spacecraft formation flying [26], the six degree-of-freedom (6DOF) FTS coordination control was proposed to suppress external disturbances for a group of spacecraft; but, the FTS coordination control was lost in the boundary layer. Moreover, the FTS tracking control strategy was presented to tackle the problem of trajectory tracking control for underactuated unmanned underwater vehicles (UUVs) [20] and Lagrangian profilers [14] with ocean current disturbances. However, the upper bound of the FTS tracking control law wasn't given. In terms of this method, more precise values of the different parameters weren't investigated [14], [20]. In order to obtain the boundary layer value of the FTS law, an FTB (finite-time boundedness) method was initially proposed for a linear system limited by uncertain parameters and unknown constant disturbances [19]. Amato's theorem [19] indicates that a system is said to be finite-time stable, if given a bound on the initial condition, once a specified time interval is fixed, its state remains within a bounded region which does not exceed a certain threshold during this specified time interval. In addition, to solve the state feedback stabilization problem of switched linear systems, a new method called "overshoot estimation in pole placements" (OEIPP) was used to estimation on the overshoots of the transition matrices [24]; however, some practical modes of switched systems were not considered in their study. Based on the OEIPP method [24], a mode-dependent average switching frequency method [25] was proposed to solve the finite-time stabilization problem of the switched nonlinear systems.

In the current work, we consider a spherical DSIB as the research object. The challenge here is that the DSIB ascends

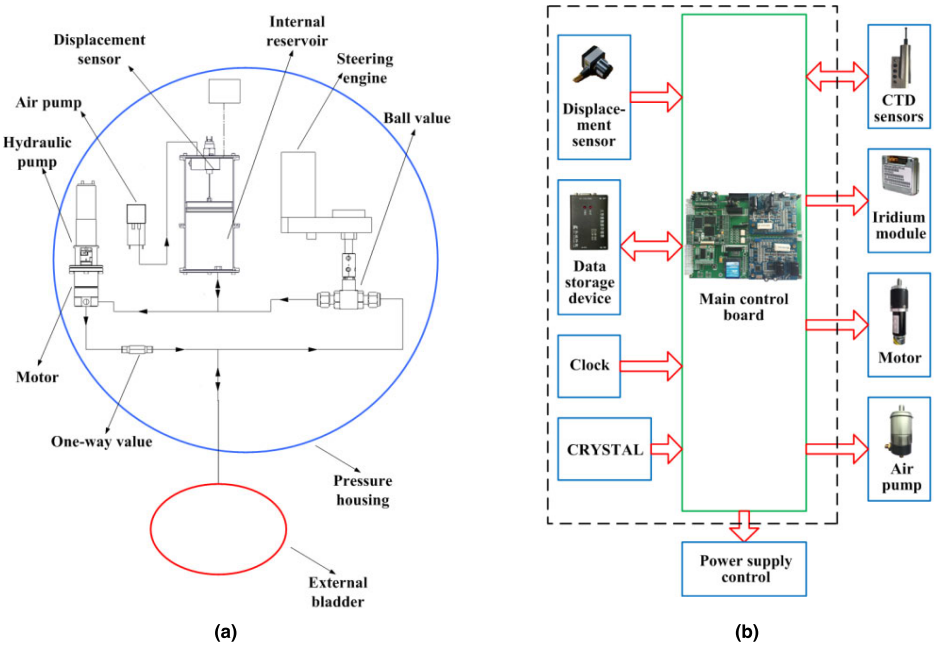

FIGURE 2. Depth control system of the DSIB. (a) Schematic of the buoyancy-driven system; (b) Schematic of the DSIB control system.

or dives at a certain speed from the initial depth to the target depth under ocean current disturbances within a finite time. Motivated by above considerations, the depth control problem of the DSIB closed-loop control system is the typical state feedback stabilization problem. Inspired by the control technique from article [24] and FTB method [19], the OEIPP method is used to establish the transition matrix of the DSIB closed-loop control system. A FTB depth control strategy with the OEIPP method is proposed to solve the depth control problem of the DSIB dynamic model within a given finite settling time. The difference from this control strategy and the conventional control method [7], [8], [13], [15], [16], [23] is that the depth error and transient time of the DSIB closed-loop control system are improved under ocean current disturbances. The upper bound of depth positioning can be determined. Meanwhile, the satisfying control effect can be obtained by carefully selecting relevant parameters. This method decreases the influence of ocean current disturbances and is suitable for solving the depth control problem. The overall organization of this paper is as follows: Section 2 describes the depth control process of the DSIB. In Section 3, a vertical dynamic model of the DSIB system is deduced under the influence of the disturbing current. In Section 4, the FTB depth control strategy with the OEIPP method is designed. The designed depth control method drives the state of the depth control system to converge to the prescribed bound in a finite time. In Section 5, relevant simulations and at-sea experiments demonstrate the applicability of the proposed depth control method to current disturbances in various scenarios. The adjustment rule of the control gains under various current disturbances within a finite time is verified. Finally, some conclusions are drawn in Section 6.

II. DEPTH CONTROL PROCESS USING BUOYANCY-DRIVEN SYSTEM

To achieve the depth control process from the sea surface to 4000 m underwater, the DSIB is equipped with a buoyancy-driven system. A schematic of the designed buoyancy-driven DSIB system is presented in Fig. 2(a). In the submerging process, the ball valve is opened by the steering engineer. Hydraulic oil is allowed to flow from the external bladder back into the internal reservoir [1], [4], [11]. As the volume of the external bladder diminishes, leading to a decrease in the buoyancy, the DSIB dives to the predefined depth. The DSIB is suspended at a target depth for the scheduled period. In the floating process, the air pump is opened to provide an appropriate pressure for the internal reservoir. Hydraulic oil is injected into the internal reservoir through a filter and a hydraulic pump which is driven by a motor. Hydraulic oil is also pumped into the external bladder through a one-way value that is closed at this time. The one-way valve can prevent backflow of the hydraulic oil through the hydraulic pump [1], [4], [11]. The buoyancy of the DSIB is increased as the volume of the external bladder expands. The external bladder is located at the exterior of the spherical hull. The volume of external bladder is measured by a displacement sensor. The DSIB ascends when the buoyancy is greater than the gravity. The depth data are collected during the ascent of the float to the surface. After the data are transmitted, a new dive will be started for the next schedule, and this process continues until the system battery runs out of power.

TABLE 1. DSIB specifications.

Description	Value
DSIB height	0.82 m
DSIB maximum width	0.54 m
Total mass of DSIB	52.39 kg
Own volume of DSIB	0.0504m^3
Maximum diving depth	4000 m
Payload capacity	Salinity, temperature, depth, pH, ORP, SVP sensors, current meter

A schematic of the DSIB control system is shown in Fig. 2(b). The control system is composed of a main control board, executive elements, and a power supply. The executive elements include CTD (conductivity, temperature, depth) sensors, an iridium module, a motor, an air pump, and a displacement sensor. The power supply is made up of multiple sets of batteries and the power is delivered to various executive elements according to the control program. The DSIB control system functions as follows: The control program is pre-written into the main control board. The control time is set. The CPU (central processing unit) works according to the control program. As per the collected depth information from the CTD sensors and the displacement information from the displacement sensor, a work or stop command is sent to each executive element. The control system is used to make cyclical operations such as diving, depth positioning, and floating. The prototype of the DSIB is shown in Fig. 3, with relevant specifications listed in Table 1.

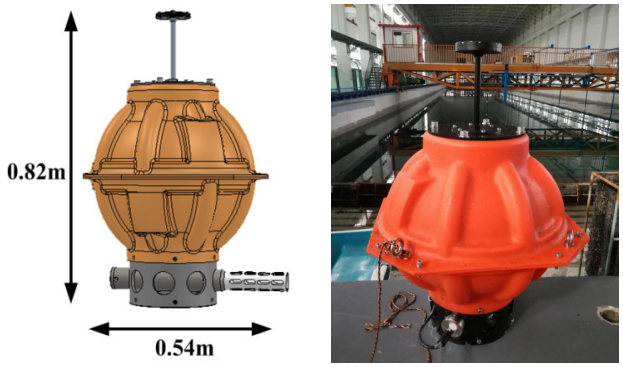

FIGURE 3. Prototype of DSIB.

III. DSIB MOTION MODELING IN VERTICAL PLANE

According to Newton's 2nd law of motion, when the DSIB is floating or submerging from the initial depth to the target depth, the acceleration of the DSIB is produced by a combination of forces, namely the weight, buoyancy, and the drag. In the aforementioned process, the DSIB is influenced by the currents all the time. While the gravity force is constant, buoyancy, drag, and current velocity change with depth. The change in the buoyancy force on the DSIB with depth is due to pressure hull deformation. Thus, the pressure hull deformation has a significant effect on the dynamic behavior of the DSIB.

A. DEFORMATION OF SPHERICAL PRESSURE HULL UNDER EXTERNAL PRESSURE

In our study, a spherical pressure hull is used in the pressure-proof structure of the DSIB. Only the volume changes induced by the deformation with increasing seawater pressure are considered. The deformation of the spherical pressure hull under seawater pressure condition slightly reduces the active buoyancy of the DSIB [3]–[6]. Thus, the deformation of the spherical pressure hull cannot be ignored in deep sea. The volume compression of the spherical pressure hull induced by the deformation at different pressure is expressed as follows [9]:

$$\Delta V = \frac{4\pi r^3 P_z}{E[r^3-(r-\delta)^3]}\left[(1-2\lambda)r^3+\frac{1+\lambda}{2}(r-\delta)^3\right] \quad (1)$$

Explanation of the parameters in (1) and their values in our study are as follows: r is the radius of the spherical pressure hull (0.216 m), λ is the Poisson's ratio (0.2), E is the modulus of elasticity on the spherical pressure hull (63 GPa), δ is the thickness of the spherical pressure hull (0.0135 m), and P_z is the pressure at the target depth $z(P_z = \rho g z,\ g = 9.8 m/s^2)$. The material used for the spherical pressure hull is glass. Substituting the values for the above parameters in (1), we obtain the following:

$$\Delta V = q\rho z \quad (2)$$

where, $q = 1.25E - 11$.

B. DISTURBANCE MODEL OF THE OCEAN CURRENT

When a DSIB is submerged in deep sea, it is influenced by several disturbance components including the currents, tides, and the sea waves [14]. Among these disturbance factors, only the effect of the currents is considered as a major factor in this study. The characteristics of the current motion acting on the DSIB mainly depend on the sea trial area. The South China Sea (15.5°N, 115.5°E and 14°N, 116°E) is selected as the sea trial area in this study.

For the deep-sea case, the currents below 200 m are small [10]. To simulate these currents and their effects on the float motion in the vertical plane, we make an assumption that the velocity of the current decreases linearly only with the increasing diving depth, and the velocity vector of current is collinear with the velocity vector of the wave. Thus, the velocity vector of the current can be taken as a graded distribution along the diving depth in the vertical plane, and

can be written [20] as

$$u = (u_0 - kz)\cos\theta \tag{3}$$

where, u is the current velocity at depth z, u_0 is the current velocity at the sea surface, k is the coefficient relative to the sea trial area, and the coefficient k is measured to be 0.00013 by a current meter in the sea trial area. θ is the angle between the current direction and the vertical direction. θ is set as 60°in this study.

C. DRAG ANALYSIS

The drag force on the DSIB is assumed to be a quadratic drag law and is expressed as follows [5], [13]:

$$R = \frac{1}{2}C_d A\rho v^2 \tag{4}$$

where, $R$is the drag force , A is the effective cross-sectional area of the DSIB, and C_d is the drag coefficient. The effective cross-sectional area can be obtained by the projection of the 3D model onto the vertical plane. In the current study, A is calculated to be 0.301 m^2, by using (4). Rearranging (1), C_d can be expressed as

$$C_d = \frac{2R}{A\rho v^2} \tag{5}$$

Different flow velocities from 0.1 m/s to 0.5 m/s are given at the inlet of the computational domain to simulate the DSIB by using the CFD (computational fluid dynamics) solver, FLUENT®6.3 in the ascending or diving process. The overall drag forces on the DSIB are calculated for both ascending and diving motions at these velocities. The corresponding drag coefficients are displayed in Tables 2 and 3.

TABLE 2. DRAG coefficient of the DSIB in the ascending process.

Motion velocity of DSIB (m/s)	0.1	0.2	0.3	0.4	0.5
Drag coefficient	0.71	0.73	0.73	0.74	0.73

TABLE 3. DRAG coefficient of the DSIB in the diving process.

Motion velocity of DSIB (m/s)	0.1	0.2	0.3	0.4	0.5
Drag coefficient	0.68	0.68	0.66	0.64	0.64

The average drag coefficients of the DSIB in ascending and the diving processes are denoted by C_{d-up} and C_{d-down}, respectively, and these are obtained by averaging the corresponding drag coefficients shown in Tables 2 and 3. These are calculated to be $C_{d-up} = 0.73$, and $C_{d-down} = 0.66$. Equation (4) shows that the drag force is nonlinear, which can be approximated to a linear expression at the velocity equilibrium point. The velocity component of the drag term is expressed as $v|v|$ instead of v^2. Considering the current velocity, u, the drag can be linearized as

$$R = \frac{1}{2}C_d A\rho(v-u)|v-u| \tag{6}$$

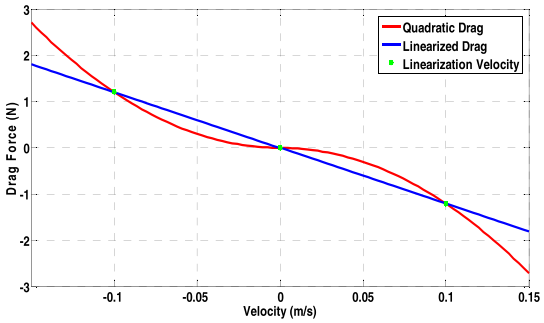

FIGURE 4. Relationship between the quadratic drag and the linearized drag.

The relationship between the quadratic and linearized drags is shown in Fig. 4. The horizontal axis is the motion velocity of the DSIB, and the vertical axis is the drag force. The drag law is approximately quadratic as indicated by the red solid line, and the linearized drag is represented by the blue solid line. Finally, the linearization velocity of the DSIB ($|v-u| = 0.1m/s$) under the current disturbances, is represented by the green point.

D. KINEMATIC EQUATION OF DSIB IN CURRENTS

The dynamic model of the DSIB in disturbing currents is considered to be nonlinear and coupled in the vertical plane. However, a linearized dynamic model can be used in this study with linear techniques. Therefore, simplifying them at the operating point based on special assumptions is necessary as follows [21]–[23]:

1) The total mass of the DSIB is constant. The center of mass and the center of buoyancy are axially collinear. The DSIB is regarded as a spherical entity in the vertical plane, and the direction of its movement is also vertical.
2) The current is not negligible in the vertical plane, and the drag force is considered to be linear.

Based on these special assumptions, the dynamic model of the DSIB is established under the current disturbances in the vertical plane. The DSIB ascends or descends at a velocity v from the initial depth to the target depth. In the above process, the relevant forces and relevant velocity vectors acting on the DSIB include buoyancy **F**, gravity **G**, drag **R**, current velocity $\mathbf{u_0}$, and motion velocity of the DSIB **v**, as illustrated in Fig. 5. The angle between the current velocity direction and the motion velocity direction of the DSIB is θ. In Fig. 5, the floating (ascending) process is represented by the region marked blue, and the submerging (diving) process is represented by the region marked red.

Based on the assumption that the DSIB reaches the predefined target depth h, where, h is a fixed value, the associated depth error is set as $\hat{z} = z - h$. This study focuses on the changes of the depth error within a finite time based on the depth control system of the DSIB. According to (3) and (6), the floating and submerging processes of the DSIB are represented by the following force equilibrium equations (7)

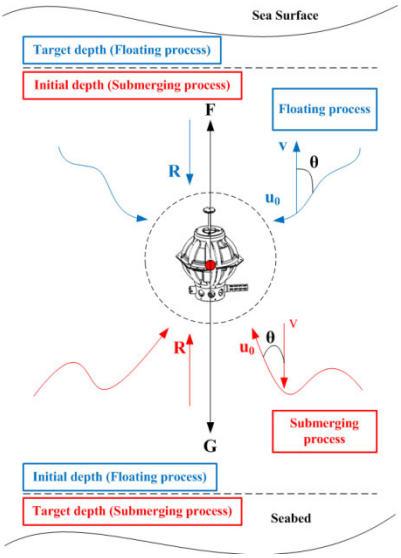

FIGURE 5. Significant forces acting on DSIB during floating (ascending) and submerging (diving) processes.

and (8), respectively. Tables 4 and 5 respectively present the dynamic variables and the non-dynamic constants.

$$\begin{cases} M(v-u)' = \rho_{(\hat{z}+h)} g(V_f - \Delta V + Q) \\ \qquad\qquad -Mg - \frac{1}{2} C_{d-up} A \rho_{(\hat{z}+h)} (v-u)\,|v-u| \\ \dot{\hat{z}} = v - (u_0 - k(\hat{z}+h))\cos\theta \end{cases} \tag{7}$$

$$\begin{cases} M(v-u)' = Mg - \rho_{(\hat{z}+h)} g(V_f - \Delta V + Q) \\ \qquad\qquad -\frac{1}{2} C_{d-down} A \rho_{(\hat{z}+h)} (v-u)\,|v-u| \\ \dot{\hat{z}} = v - (u_0 - k(\hat{z}+h))cos\theta \end{cases} \tag{8}$$

According to (7) and (8), the state-space equation of the DSIB system can be obtained as follows:

1) IN THE ASCENDING PROCESS

$$\begin{bmatrix} \dot{v} \\ \dot{\hat{z}} \end{bmatrix} = \begin{bmatrix} R_1^a & R_2^a \\ 1 & R_3^a \end{bmatrix} \begin{bmatrix} v \\ \hat{z} \end{bmatrix} + \begin{bmatrix} R_4^a \\ 0 \end{bmatrix} Q + \begin{bmatrix} R_2^a \\ R_3^a \end{bmatrix} h + \begin{bmatrix} R_5^a \\ R_6^a \end{bmatrix} \tag{9}$$

where

$$R_1^a = -\frac{C_{d-up} A \rho_{(\hat{z}+h)}\,|v-u|}{2M} - k\cos\theta,$$

$$R_2^a = -k\cos\theta \frac{C_{d-up} A \rho_{(\hat{z}+h)}\,|v-u|}{2M} - k^2\cos^2\theta - \frac{\rho_{(\hat{z}+h)}^2 gq}{M},$$

$$R_3^a = k\cos\theta, R_4^a = \frac{\rho_{(\hat{z}+h)} g}{M}, \quad R_6^a = -u_0\cos\theta,$$

$$R_5^a = u_0\cos\theta \frac{C_{d-up} A \rho_{(\hat{z}+h)}\,|v-u|}{2M} + ku_0\cos^2\theta + \frac{\rho_{(\hat{z}+h)} g V_f}{M} - g.$$

2) IN THE DIVING PROCESS

$$\begin{bmatrix} \dot{v} \\ \dot{\hat{z}} \end{bmatrix} = \begin{bmatrix} R_1^d & R_2^d \\ 1 & R_3^d \end{bmatrix} \begin{bmatrix} v \\ \hat{z} \end{bmatrix} + \begin{bmatrix} R_4^d \\ 0 \end{bmatrix} Q + \begin{bmatrix} R_2^d \\ R_3^d \end{bmatrix} h + \begin{bmatrix} R_5^d \\ R_6^d \end{bmatrix} \tag{10}$$

where

$$R_1^d = -\frac{C_{d-down} A \rho_{(\hat{z}+h)}\,|v-u|}{2M} - k\cos\theta,$$

$$R_d^2 = -k\cos\theta \frac{C_{d-down} A \rho_{(\hat{z}+h)}\,|v-u|}{2M} - k^2\cos^2\theta + \frac{\rho_{(\hat{z}+h)}^2 gq}{M},$$

$$R_3^d = k\cos\theta, \quad R_4^d = -\frac{\rho_{(\hat{z}+h)} g}{M}, R_6^d = -u_0\cos\theta,$$

$$R_5^d = g + u_0\cos\theta \frac{C_{d-down} A \rho_{(\hat{z}+h)}\,|v-u|}{2M} + ku_0\cos^2\theta - \frac{\rho_{(\hat{z}+h)} g V_f}{M}$$

According to the state-space equations (9) and (10), the motion state vector of the DSIB is $x(t) = \begin{bmatrix} v & \hat{z} \end{bmatrix}^T$, where v and $\hat{z}$ are state variables. The predefined target depth h is usually viewed as a constant. Thus, the state–space equations of the DSIB system (9) and (10) can be considered as the following time-invariant linear system:

$$\dot{x}(t) = \boldsymbol{A}x(t) + \boldsymbol{B}\boldsymbol{Q} + \boldsymbol{C}, \quad x(0) = x_0 \tag{11}$$

The state–space equation of the DSIB system (11) is the dynamic open-loop system expression.

In the state–space equation of the ascending process:

$$\boldsymbol{A} = \begin{bmatrix} R_1^a & R_2^a \\ 1 & R_3^a \end{bmatrix}, \quad \boldsymbol{B} = \begin{bmatrix} R_4^a \\ 0 \end{bmatrix}, \quad \boldsymbol{C} = \begin{bmatrix} R_2^a \\ R_3^a \end{bmatrix} h + \begin{bmatrix} R_5^a \\ R_6^a \end{bmatrix}$$

In the state–space equation of the diving process:

$$\boldsymbol{A} = \begin{bmatrix} R_1^d & R_2^d \\ 1 & R_3^d \end{bmatrix}, \quad \boldsymbol{B} = \begin{bmatrix} R_4^d \\ 0 \end{bmatrix}, \quad \boldsymbol{C} = \begin{bmatrix} R_2^d \\ R_3^d \end{bmatrix} h + \begin{bmatrix} R_5^d \\ R_6^d \end{bmatrix}$$

where, $\boldsymbol{A} \in \boldsymbol{R}^{2\times 2}$, $\boldsymbol{B} \in \boldsymbol{R}^{2\times 1}$, $\boldsymbol{C} \in \boldsymbol{R}^{2\times 1}$ are the given matrices, $\boldsymbol{Q}$ is the control input, and $\boldsymbol{C}$ is the disturbances matrix. In the given state variables of the DSIB model, the depth z and hydraulic oil volume of the external bladder $\boldsymbol{Q}$ can be measured directly.

Considering the DSIB system (11) to be unstable under the currents, a state feedback controller $\boldsymbol{K}$ is designed in the following form:

$$\boldsymbol{Q}(t) = \boldsymbol{K}x(t) \tag{12}$$

where, $\boldsymbol{K} \in \boldsymbol{R}^{2\times 1}$.

The obtained state feedback control gains $\boldsymbol{K}$ make the closed-loop depth control system of the DSIB stable. The closed-loop depth control system state equation by connecting (11) and (12) is as follows:

$$\dot{x}(t) = (\boldsymbol{A} + \boldsymbol{B}\boldsymbol{K})x(t) + \boldsymbol{C}, x(0) = x_0 \tag{13}$$

TABLE 4. Dynamic variables of the DSIB.

Parameter	Units	Description	Parameter	Units	Description
G	N	Weight	$\hat{z}$	m	Depth error
F	N	Buoyancy	v	m/s	Motion velocity of the DSIB
R	N	Drag	$(v-u)'$	m/s^2	Acceleration of the DSIB in currents
θ	°	Current direction in vertical plane	u	m/s	current velocity
$\rho_{\hat{z}+h}$	kg/m^3	Seawater density at a set depth scope	V	m^3	Total volume of the DSIB
z	m	Depth of the DSIB in currents	ΔV	m^3	The volume compression of the DSIB
h	m	Target depth	Q	m^3	Hydraulic oil volume of external bladder

TABLE 5. Non-dynamic constants of the DSIB.

Parameter	Value	Units	Description
M	52.39	kg	Total mass of the DSIB
g	9.8	m/s^2	Acceleration due to gravity
V_f	0.0504	m^3	Volume of the DSIB
$C_{d\text{-}up}$	0.77		Drag coefficient as the DSIB ascending
$C_{d\text{-}down}$	0.7		Drag coefficient as the DSIB diving
A	0.301	m^2	Projected area of hull
k	0.00013		Current coefficient relative to the sea trial area

IV. FTB DEPTH METHOD DESIGN FOR THE DSIB CLOSED-LOOP DEPTH CONTROL SYSTEM

Before the DSIB is deployed, the control time and control gains of the depth control system are usually set to achieve the depth control process of the DSIB. Owing to the disturbance of the external current, the DSIB cannot be effectively controlled in this process, and as a result, both convergence and divergence states may occur. To observe the transient state of the DSIB, it is necessary to study the relationship between the control gains and current disturbance in a finite time, so that the DSIB can be guaranteed to achieve the depth control in a finite time under the influence of the external currents. To solve the transient stability problem for the time-invariant linear system given by (13) over a finite time interval [0,T], the concept of FTB is introduced. Referring to the relevant definition of FTB [19], the same for a closed-loop depth control system can be defined as the following engineering problem:

Definition 1: In the ascending or diving process, consider three positive constants c_1, c_2, and T, and a positive definite matrix $\boldsymbol{R} > 0$. c_1 is the area scope where the DSIB is located at the initial time. c_2 is the area scope where the DSIB is allowed to locate over a finite-time interval [0,T]. At the initial time, the motion state vector of the DSIB is $x_0 = \begin{bmatrix} v_0 & \hat{z}_0 \end{bmatrix}^T$. At time t, the motion state vector of the DSIB is $x(t) = \begin{bmatrix} v_t & \hat{z}_t \end{bmatrix}^T$.Considering the closed-loop depth control system formed from time-invariant linear system (13), if

$$x_0^T R x_0 \le c_1 \Rightarrow x^T(t) R x(t) < c_2, \quad \forall t \in [0, T] \tag{14}$$

then, the closed-loop depth control system (13) is characterized by FTB, which is given with respect to (c_1, c_2, T, $\boldsymbol{R}$).

On the basis of Definition 1, a sufficient condition for the solution of this engineering problem is given by the following theorem:

Theorem 1: Given three positive constants c_2, T, and M, and a positive definite matrix $\boldsymbol{R} > 0$, for any $\lambda_s > 0$, if

$$\lambda_{\max}(\boldsymbol{R})(M\lambda_s^{n-1}e^{-\lambda_s T}\,\|x(0)\| + \|\boldsymbol{C}\|\,T)^2 \le c_2 \tag{15}$$

where, $\lambda_{max}(R)$ is the maximum eigenvalue of the positive definite matrix R. Let n be the order of the positive definite matrix R. Here, M is a constant, which is greater than 0 and is independent of λ_s, and can be estimated precisely in terms of A_i, B_i, and $n.\lambda_s$ is the decay rate; T is a finite time interval; c_2 is the area scope where the DSIB is allowed to be located over a finite-time interval [0,T]; $\| x_{(0)} \|$ is the norm of the DSIB system state $x_{(t)}$ at the initial time; $\| C \|$ is the norm of the constant matrix for the disturbances of the closed-loop depth control system (13). Then, the closed-loop depth control system is finite-time bounded with respect to (c_2, T, $\boldsymbol{R}$).

Proof:

To solve the FTB problem for the closed-loop depth control system represented by (13), the criteria need be established for the finite-time transformation matrix. Equation (13) can be rewritten as follows:

$$x(t) = e^{(A+BK)}x(0) + \int_0^t \boldsymbol{C}\,dt \tag{16}$$

A new method, called ''overshoot estimation in pole placements'' is used to estimate the transition matrix $e^{(A_i \mathcal{C} B_i K_i)t}$.

Let $\boldsymbol{A_i} \in \boldsymbol{R}^{2\times 2}$ and $\boldsymbol{B_i} \in \boldsymbol{R}^{2\times 1}$ be constant matrices. If the pair ($\boldsymbol{A}$, $\boldsymbol{B}$) is controllable, then, for any $\lambda_s > 0$, a matrix $\boldsymbol{K_i} \in \boldsymbol{R}^{2\times 1}$ exists, which satisfies [24]

$$\left\| e^{(A_i + B_i K_i)t} \right\| \le M\lambda_s^{n-1}e^{-\lambda_s t}, \quad t \ge 0 \tag{17}$$

where, $M > 0$ is a constant. $M = n^{n+1}\,|\boldsymbol{F_1}|\left|\boldsymbol{F_1^{-1}}\right| N_0$, which is independent of λ_s and can be estimated precisely in terms of A_i, B_i, and n. Here, n is the order of the matrix A_i and λ_s is

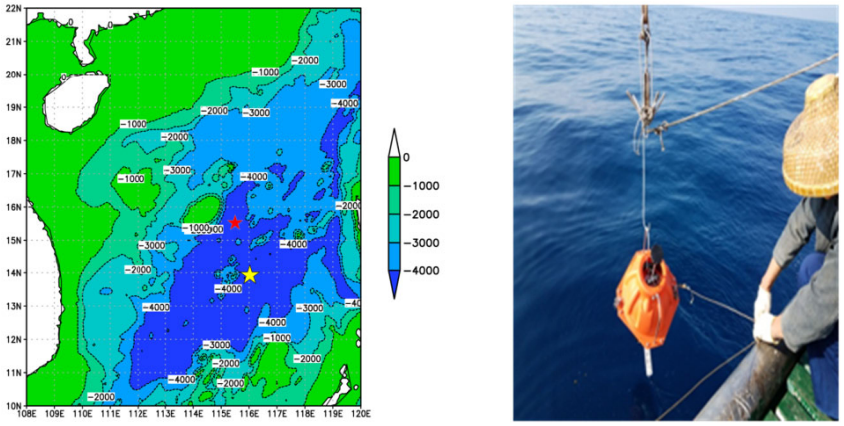

(a) (b)

FIGURE 6. Planned mission scenario of the DSIB: (a) Position of the DSIB deployed in south china Sea; (b) Deployment process of the DSIB.

the decay rate.

$$\boldsymbol{F_1} = [\boldsymbol{A}^{n-1}\boldsymbol{B}\cdots\boldsymbol{A}\boldsymbol{B}\ \boldsymbol{B}]\begin{bmatrix} 1 & 0 & \cdots & 0 \\ a_{n-1} & 1 & \cdots & 0 \\ \vdots & \ddots & \ddots & \vdots \\ a_1 & \cdots & a_{n-1} & 1 \end{bmatrix},$$

$$N_0 \triangleq \frac{n^{n(n-1)/2}}{\prod_{1\le i\le n-2} i!} \tag{18}$$

If (17) states a sufficient condition for the FTB of the closed-loop depth control system in the form (13), then

$$\left\| e^{(\boldsymbol{A}+\boldsymbol{BK})t} \right\| \le M\lambda_s^{n-1}e^{-\lambda_s t}, \quad t \ge 0 \tag{19}$$

On the other hand,

$$\lambda_{min}(\boldsymbol{R})\,\|x(t)\|^2 \le x^T(t)\boldsymbol{R}x(t) \le \lambda_{\max}(\boldsymbol{R})\,\|x(t)\|^2 \tag{20}$$

where $\lambda_{max}(\boldsymbol{R})$ is the maximum eigenvalue of the positive definite matrix $\boldsymbol{R}$.

$$\|x(t)\| = \left\| e^{(A+BK)}x(0) + \int_0^t Cdt \right\| \le M\lambda_s^{n-1}e^{-\lambda_s t}\,\|x(0)\| + \|C\|\int_0^t dt \tag{21}$$

Based on the definition of the FTB$t \propto T$, the closed-loop depth control system (13) can be rewritten as follows:

$$\|x(t)\| \le M\lambda_s^{n-1}e^{-\lambda_s t}\,\|x(0)\| + \|C\|\,T \tag{22}$$

Thus, we have

$$x^T(t)Rx(t) \le \lambda_{\max}(R)(M\lambda_s^{n-1}e^{-\lambda_s T}\,\|x(0)\| + \|C\|\,T)^2 \le c_2 \tag{23}$$

Thus, the proof of Theorem 1 is completed.

In summary, a state feedback controller (12) exists such that the closed-loop depth control system (13), under the external disturbances is bounded over a finite-time interval [0,T].

V. RESULTS AND ANALYSIS

To illustrate the theoretical results obtained in the previous sections, both simulations and sea trials were conducted to evaluate the performance of the proposed depth control method. During THE SEA TRIAL, THE DSIB WAS CONSIDERED TO HAVE BEEN DEPLOYED IN TWO POSITION OF THE SOUTH CHINA SEA (15.5°N, 115.5°E and 14°N, 116°E) (see Fig. 6). The DSIB was equipped with a CTD sensor (Sea-Bird Electronics, Inc., SBE 49) to measure the depth, conductivity and temperature. These measured values were used to calculate the seawater density. When the depth was between 600 m and 800 m, the seawater density range was between 1029.9kg/m^3 and 1030.8kg/m^3. When the depth was between 2500 m and 2800 m, the seawater density range was between 1039.4kg/m^3 and 1040.5kg/m^3.The measured depth rate was used to estimate the motion velocity of the DSIB at the initial time. The mean vertical velocity of the DSIB at the initial time was approximately 0.5 m/s in both the ascending and diving processes in this study. The current velocity data used in this work came from real measurements at location with an HS-Engineers ISMart 6000 m current meter. The current velocity at the sea surface was respectively approximately 0.78m/s and 1.5m/s in two position of the South China Sea (15.5°N, 115.5°E and 14°N, 116°E).

A. SIMULATION RESULTS AND ANALYSIS

Relevant simulations have been conducted to validate the proposed depth control method under the current disturbances. To study the relationship between the control gains and the current disturbances in the proposed depth control method, the simulations are divided into those in shallow water (restricted to a depth above 2000 m, and henceforth referred to as scenario 1) and those in deep water (restricted to a depth between 2000 m and 4000 m, and henceforth referred to as scenario 2). Furthermore, two cases are considered in each of these scenarios:

a. *Identical control gains are used in the FTB method under different current disturbances as the DSIB ascends or dives.*
b. *Varied control gains are used in the FTB method under identical current disturbances as the DSIB ascends or dives.*

1) SCENARIO 1: RESTRICTION TO ABOVE 2000M

The DSIB ascends at a speed of 0.5 m/s at the initial time from an initial depth of 800 m to a target depth of 600 m. At the initial time, the motion state vector of the DSIB is $x(0) = \begin{bmatrix} 0.5 & 200 \end{bmatrix}^T$. In the above process, the control gains $\boldsymbol{K}$ make the closed-loop depth control system converge to an allowable depth error of 15 m around the target depth within 2000 s under various current disturbances.

According to Scenario 1, the non-dynamic constants are substituted into (9), and the initial conditions are as follows:

$$\boldsymbol{A} = \begin{bmatrix} -0.23 & 1.73E-5 \\ 1 & 0.000065 \end{bmatrix}, \quad \boldsymbol{B} = \begin{bmatrix} 192.67 \\ 0 \end{bmatrix},$$
$$x(0) = \begin{bmatrix} 0.5 \\ 200 \end{bmatrix}, \quad h\ 600.$$

a. *Identical control gains* $K = [-10, -1]$ are used in the FTB method under different current disturbances as the DSIB ascends.

Based on the proposed Theorem 1, and [24], the calculated values of c_2, T, and M are 44100, 2000, and 16, respectively. Let the state feedback control gains be $K = [k_1, k_2]$. From $|\lambda \boldsymbol{I} - (\boldsymbol{A} + \boldsymbol{BK})|$, the eigenvalue, λ is < 0. For the calculated control gains $\boldsymbol{K} = [-10, -1]$, the closed-loop depth control system equations are (24) and (25) respectively, and are finite-time bounded.

When $u_0 = 0.78$m/s,

$$\begin{bmatrix} \dot{v} \\ \dot{\hat{z}} \end{bmatrix} = \begin{bmatrix} -1926.93 & -192.67 \\ 1 & 0.000065 \end{bmatrix} \begin{bmatrix} v \\ \hat{z} \end{bmatrix} + \begin{bmatrix} -0.01662 \\ -0.351 \end{bmatrix} \quad (24)$$

When $u_0 = 1.5$m/s,

$$\begin{bmatrix} \dot{v} \\ \dot{\hat{z}} \end{bmatrix} = \begin{bmatrix} -1926.93 & -192.67 \\ 1 & 0.000065 \end{bmatrix} \begin{bmatrix} v \\ \hat{z} \end{bmatrix} + \begin{bmatrix} 0.08838 \\ -0.711 \end{bmatrix} \quad (25)$$

b. *Varied control gains are used under identical current disturbances ($u_0 = 0.78$ m/s) as the DSIB ascends.*

Based on the proposed Theorem 1, in a similar way, the calculated values of c_2, T, and M are 44100, 2000, and 16, respectively. For the calculated control gains $\boldsymbol{K} = [-10, -0.5]$, the closed-loop depth control system equation is (26) and is finite-time bounded.

$$\begin{bmatrix} \dot{v} \\ \dot{\hat{z}} \end{bmatrix} = \begin{bmatrix} -1926.93 & -96.335 \\ 1 & 0.000065 \end{bmatrix} \begin{bmatrix} v \\ \hat{z} \end{bmatrix} + \begin{bmatrix} -0.01662 \\ -0.351 \end{bmatrix} \quad (26)$$

2) SCENARIO 2: RESTRICTION TO DEPTH BETWEEN 2000 M AND 4000 M

The DSIB dives at a speed of 0.5 m/s at the initial time from the initial depth of 2500 m to the target depth of 2800 m. At the initial time, the motion state vector of the DSIB is $x(0) = \begin{bmatrix} 0.5 & 300 \end{bmatrix}^T$. In the above process, the calculated control gains $\boldsymbol{K}$ make the closed-loop depth control system converge to an allowable depth error of 20 m around the target depth within 2000 s under the current disturbances.

According to the Scenario 2, the non-dynamic constants are substituted into (10), and the initial conditions are as follows:

$$\boldsymbol{A} = \begin{bmatrix} -0.21 & -1.11E-5 \\ 1 & 0.000065 \end{bmatrix}, \quad \boldsymbol{B} = \begin{bmatrix} -194.54 \\ 0 \end{bmatrix},$$
$$x(0) = \begin{bmatrix} 0.5 \\ 300 \end{bmatrix}, \quad h = 2800.$$

a. *Identical control gains* $\boldsymbol{K}$*= [10,0.5] are used in the FTB method under different current disturbances as the DSIB dives.*

Based on the proposed Theorem 1, and according to the reference [24], the calculated values of c_2, T, and M are 96100, 2000, and 15.75, respectively. Let state feedback control gains be $\boldsymbol{K} = [k_1, k_2]$. From $|\lambda \boldsymbol{I} - (\boldsymbol{A} + \boldsymbol{BK})|$, the eigenvalue, λ is <0. For the calculated control gains $\boldsymbol{K} = [10, 0.5]$, the closed-loop depth control system equations are (27) and (28), respectively, and these are finite-time bounded.

When $u_0 = 0.78$m/s,

$$\begin{bmatrix} \dot{v} \\ \dot{\hat{z}} \end{bmatrix} = \begin{bmatrix} -1945.61 & -97.27 \\ 1 & 0.000065 \end{bmatrix} \begin{bmatrix} v \\ \hat{z} \end{bmatrix} + \begin{bmatrix} 0.10808 \\ -0.208 \end{bmatrix} \quad (27)$$

When $u_0 = 1.5$m/s,

$$\begin{bmatrix} \dot{v} \\ \dot{\hat{z}} \end{bmatrix} = \begin{bmatrix} -1945.61 & -97.27 \\ 1 & 0.000065 \end{bmatrix} \begin{bmatrix} v \\ \hat{z} \end{bmatrix} + \begin{bmatrix} 0.18538 \\ -0.568 \end{bmatrix} \quad (28)$$

b. *Varied control gains are used under the identical current disturbances ($u_0 = 0.78$ m/s) as the DSIB dives.*

Based on the proposed Theorem 1, in a similar way, the calculated values of c_2, T, and M are 96100, 2000, and 15.75, respectively. For the calculated control gains $\boldsymbol{K} = [10, 0.25]$ the closed-loop depth control system equation is (29), and is finite-time bounded.

$$\begin{bmatrix} \dot{v} \\ \dot{\hat{z}} \end{bmatrix} = \begin{bmatrix} -1926.93 & -48.635 \\ 1 & 0.000065 \end{bmatrix} \begin{bmatrix} v \\ \hat{z} \end{bmatrix} + \begin{bmatrix} 0.10808 \\ -0.208 \end{bmatrix} \quad (29)$$

Figs. 7 and 8 show the state trajectories of the closed-loop depth control systems in the ascending and diving processes, respectively. The horizontal axis is the time, and the vertical axis is the motion states of the DSIB. The motion states of the DSIB consists of the motion velocity of the DSIB v and the depth error $\hat{z}$. As shown in Figs. 7(a) and 8 (a), identical control gains are used in the FTB method under different current disturbances. The identical control gains restrain the chattering of the current disturbances in both the ascending and diving processes. With the same control gains, the solid lines represent the state trajectories of the closed-loop depth control systems (24) and (27) under a current velocity of 0.78 m/s, while the dotted lines represent the state trajectories of the closed-loop depth control systems (25) and (28) under a current velocity of 1.5 m/s. Figs. 7(b) and 8 (b) show the results for the case *b*, where the FTB method is achieved by adjusting the control gains under identical current disturbances. The chattering of the current disturbances

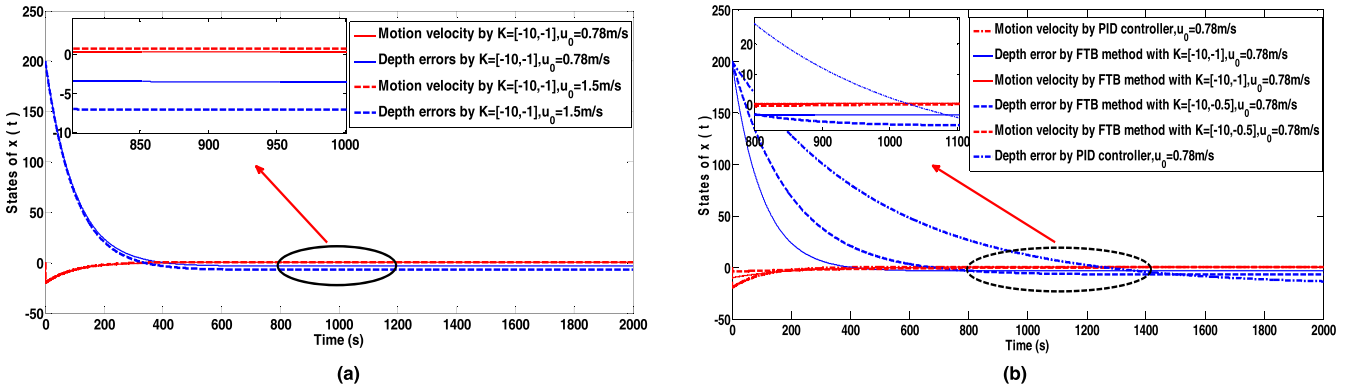

FIGURE 7. State trajectories of the closed-loop depth control system in ascending process: (a) Identical control gains used in different current disturbances; (b) Different control gains and PID controller used in identical current disturbances.

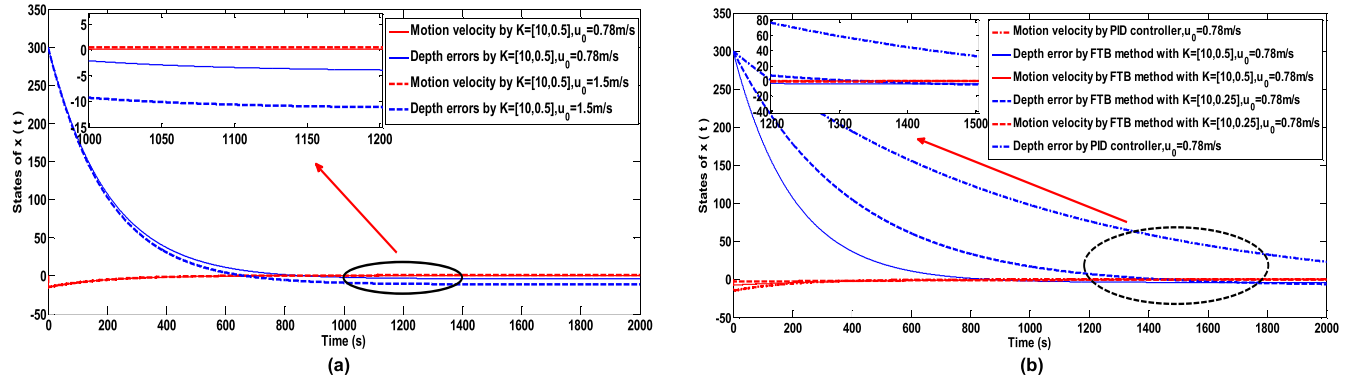

FIGURE 8. State trajectories of the closed-loop depth control system in diving process: (a) Identical control gains used in different current disturbances; (b) Different control gains and PID controller used in identical current disturbances.

is restrained both in the ascending and diving processes. Under an identical current velocity of 0.78 m/s, the solid lines represent the state trajectories of the closed-loop depth control systems (24) and (27) with the control gains $\boldsymbol{K} = [-10, -1]$ and $\boldsymbol{K} = [10,0.5]$, respectively. The dotted lines represent the state trajectories of the closed-loop depth control systems (26) and (29) with the control gains $\boldsymbol{K} = [-10, -0.5]$ and $\boldsymbol{K} = [10,0.25]$, respectively. A contrast simulation is designed to verify the performance of the FTB method compared to that of a standard PID controller. As shown in Figures 7 (b) and 8 (b), FTB method and standard PID controller are used in the depth control under identical current disturbances. The both control method restrain the chattering of the current disturbances in both the ascending and diving processes. In order to realize the depth control of the DSIB under a current velocity of 0.78m/s in the ascending process, the relevant parameters of the standard PID controller are established by a trial-and-error method as 5, 0.5, and 20 for k_p, k_i, and k_d, respectively. In the diving process, the relevant parameters of the standard PID controller are set as 5, 0.2, and 30 for k_p, k_i, and k_d, respectively. The dot dash lines represent the state trajectories of the closed-loop depth control systems with the PID controller in the ascending and diving processes, respectively.

The depth simulation results for the closed-loop depth control system are illustrated in Figure 9. In the ascending process, the proposed FTB depth control method enables the DSIB to reach the desired depth error of a target depth of 600 m under current disturbances within 1200 s, and the desired depth error is less than 15 m. In the diving process, the FTB depth controller takes about 1800 s to reach a target depth of 2800 m under current disturbances, and the desired depth error is less than 15 m.

The key results of the simulations in the ascending and diving processes are listed in Table 6. The depth error and transient time are used to describe the performance of the depth positioning. The maximum allowable error of depth positioning based on the actual hydrographic survey is usually within 50 m [30]. The simulation control time is set to 2000 s. For the standard PID controller and FTB method, the generated depth error and transient time meet the desired requirement in the ascending and diving process, respectively. Thus, the closed-loop depth control systems (24), (25), and (26) are finite-time bounded in the ascending process,

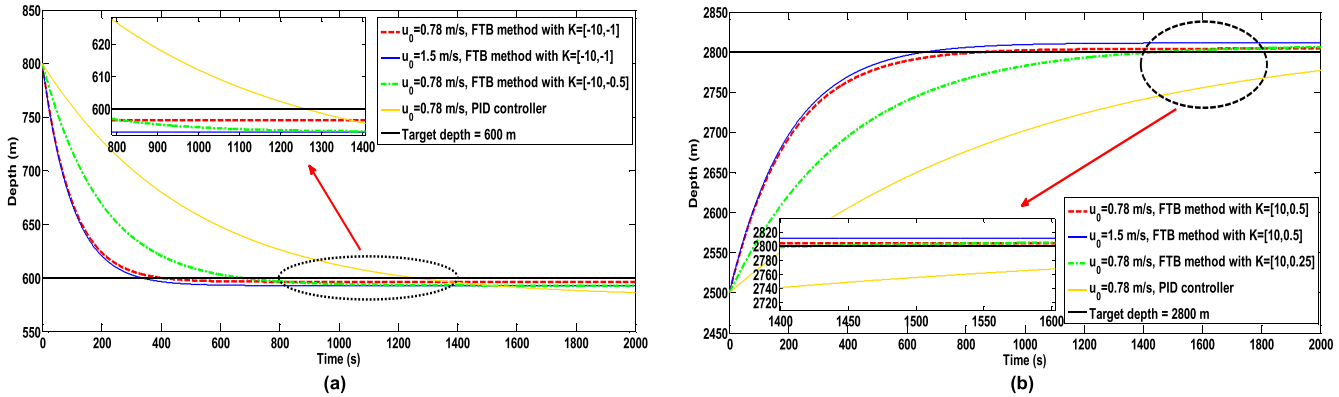

FIGURE 9. Depth simulation results for the closed-loop depth control system: (a) In ascending process; (b) In diving process.

TABLE 6. Comparison of key simulation results in ascending and diving process.

Direction of motion	Simulation setup	Current velocity (m/s)	Controller parameters setup	Transient time (s)	Depth error (m)
Ascending process	$\boldsymbol{A}=\begin{bmatrix}-0.23 & 1.73\text{E}-5\\ 1 & 0.000065\end{bmatrix}$, $\boldsymbol{B}=\begin{bmatrix}192.67\\ 0\end{bmatrix}$, $x(0)=\begin{bmatrix}0.5\\ 200\end{bmatrix}$, h=600, c_2=44100,T=2000, M=16	u_0=0.78	$\boldsymbol{K}$=[−10, −1]	826	3.6
		u_0= 1.5		902	7.6
		u_0=0.78	$\boldsymbol{K}$=[−10, −0.5]	1162	6.4
	PID controller		k_p=5, k_i=0.5,k_d=20	1456	9.2
Diving process	$\boldsymbol{A}=\begin{bmatrix}-0.21 & -1.11\text{E}-5\\ 1 & 0.000065\end{bmatrix}$, $\boldsymbol{B}=\begin{bmatrix}-194.54\\ 0\end{bmatrix}$, $x(0)=\begin{bmatrix}0.5\\ 300\end{bmatrix}$, h=2800, c_2=96100,T=2000, M=15.75	u_0=0.78	$\boldsymbol{K}$=[10, 0.5]	1268	4.2
		u_0= 1.5		1335	8.8
		u_0=0.78	$\boldsymbol{K}$=[10, 0.25]	1752	5.8
	PID controller		k_p=5, k_i=0.2,k_d=30	1885	11.7

and the closed-loop depth control systems (27), (28), and (29) are finite-time bounded in the diving process. In Table 6, we can see that, under the same current velocity of 0.78 m/s in the ascending process, by employing the control gains $\boldsymbol{K} = [-10, -1]$ compared to the control gains $\boldsymbol{K} = [-10, -0.5]$, the transient time is reduced from 1162 s to 826 s and the depth error is reduced from 6.4 m to 3.6 m. The state trajectories for the diving process and the ascending process are similar. Under the same current velocity of 0.78 m/s, the transient time and depth error with the control gains $\boldsymbol{K} =$ [10,0.5] are 1268 s and 4.2 m respectively, while the transient time and depth error with the control gains $\boldsymbol{K} = [10,0.25]$ are 1752 s and 5.8 m, respectively. It is clear that various transient states are obtained by adjusting the control gains under the same current velocity of 0.78 m/s in the ascending and diving process. However, with the identical control gains, the transient state under a current velocity of 0.78 m/s is more stable than that under a current velocity of 1.5 m/s. Furthermore, under the current velocity of 0.78 m/s, the FTB method takes about less time to reach the desired depth, which is faster than the standard PID controller in the ascending and diving process. After the steady state is attained, depth error are analyzed. The depth error is less for the FTB method than that for the standard PID controller. In summary, the transient state for the FTB method is more stable than that for the standard PID controller, which means that the proposed controller is significantly better than the standard PID controller. In addition, an adjustment rule of the control gains under identical current disturbances within a finite time is obtained through the simulation.

Figs. 10 and 11 show the phase plots of state x(t). The horizontal axis is the motion velocity of the DSIB v, and the vertical axis is the depth error $\hat{z}$.The inner circle c_1 is the area scope where the DSIB is located at the initial time, and the outer circle c_2 is the area scope where the DSIB is allowed to locate over a finite-time interval [0, T].

According to Case *a*, the phase plot of state x(t) is shown in Figs. 10(a) and 11 (a). With the same control gains, the red dotted line represents the phase trajectory of the state of the closed-loop depth control system represented by (24) and (27), under a current velocity of 0.78 m/s, while the blue solid line represents the phase trajectory of the state of the closed-loop depth control system represented by (25) and (28), under a current velocity of 1.5 m/s. In both the ascending and diving processes, the states do not exceed the outer circle c_2 when the initial states are restricted to the inner

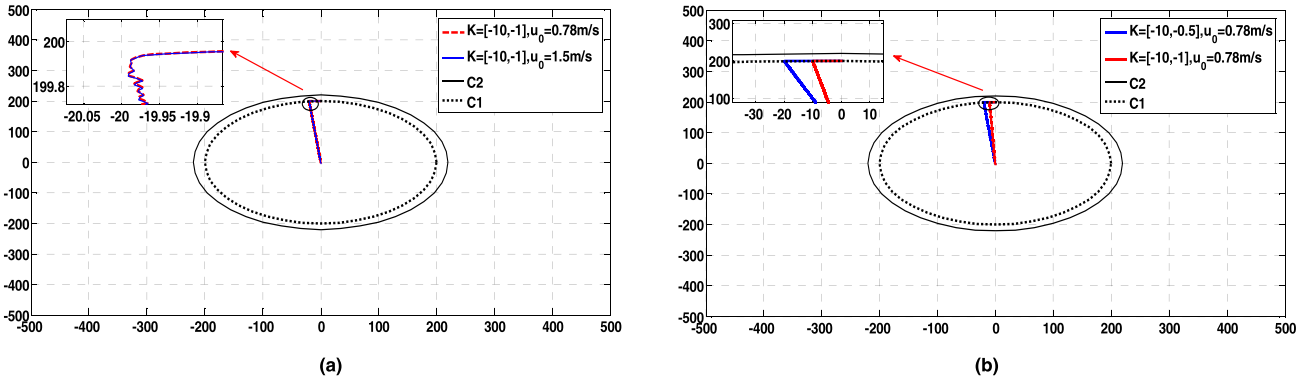

FIGURE 10. Phase plot of state x(t) in ascending process: (a) Identical control gains used in different current disturbances; (b) Different control gains used in identical current disturbances.

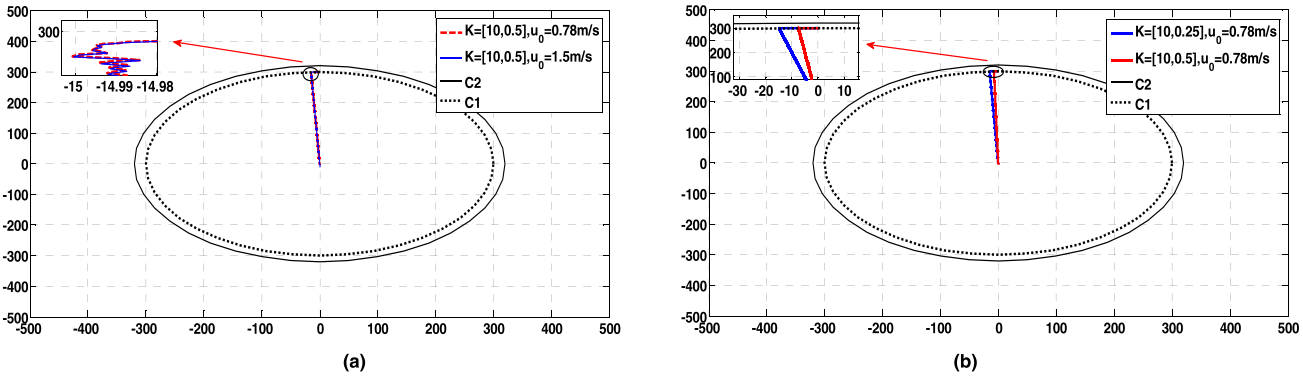

FIGURE 11. Phase plot of state x(t) in diving process: (a) Identical control gains used in different current disturbances; (b) Different control gains used in identical current disturbances.

circle c_1. The terminal states satisfy the requirements under different current disturbances. It is evident that the phase trajectories of the states with identical control gains under different current disturbances are basically the same.

According to Case *b*, the phase plot of state $x(t)$ is shown in Figs. 10(b) and 11 (b). Under an identical current velocity of 0.78 m/s, the red dotted line represents the phase trajectory of state of the closed-loop depth control system represented by (24) and (27) with the control gains $\boldsymbol{K} = [-10, -1]$ and $\boldsymbol{K} = [10, 0.5]$, respectively. The blue solid lines represent the phase trajectory of state of the closed-loop depth control system represented by (26) and (29) with the control gains $\boldsymbol{K} = [-10, -0.5]$ and $\boldsymbol{K} = [10, 0.25]$, respectively. In both the ascending and diving processes, the states do not exceed the outer circle c_2 when the initial states are restricted to the inner circle c_1. The terminal states satisfy the requirements with different control gains. The plots also reveal that the variable degree of the convergence rate is reflected by the phase trajectory of the states, when adjusting the control gains under identical current disturbances.

B. AT-SEA EXPERIMENTAL RESULTS AND ANALYSIS

To verify the effectiveness of the aforementioned simulations, the proposed depth control method was applied in a few experimental scenarios to steer the DSIB between two given positions. In the sea trial, the experiment process was as follows:

Step 1: Before the DSIB was launched, the depth control time and control gains of the depth control system were set for several experimental scenarios. The depth control time was set to 2000 s for the depth control process in this study.

Step 2: To enable the DSIB to produce a certain initial velocity at the initial depth, determining a predefined depth was necessary. The difference value between the predefined and initial depths was approximately 10–20 m. When the DSIB was deployed, the DSIB dove to the neighborhood of the predefined depth and was suspended at the neighborhood of the predefined depth. The predefined depth was measured by the CTD sensors.

Step 3: The buoyancy-driven system began to operate. The DSIB began to ascend or it dove from the predefined depth to the initial depth. When the DSIB ascended or dove to the initial depth, the mean motion velocity of the DSIB at the current time was approximately 0.5 m/s. The current time was then recorded as the initial time. At the initial time, the depth control system commenced operation according to the depth control time and control gains.

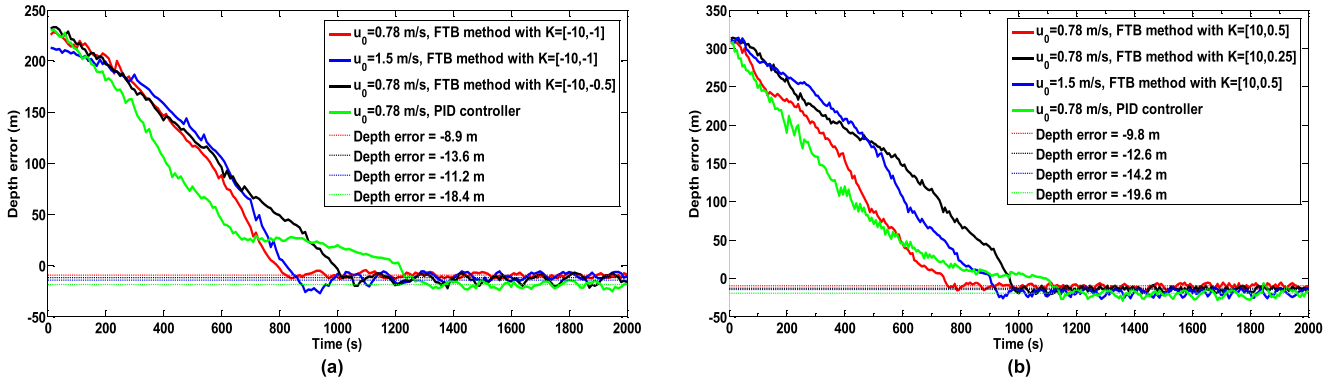

FIGURE 12. Depth error experimental results for the closed-loop depth control system: (a) In ascending process, (b) In diving process.

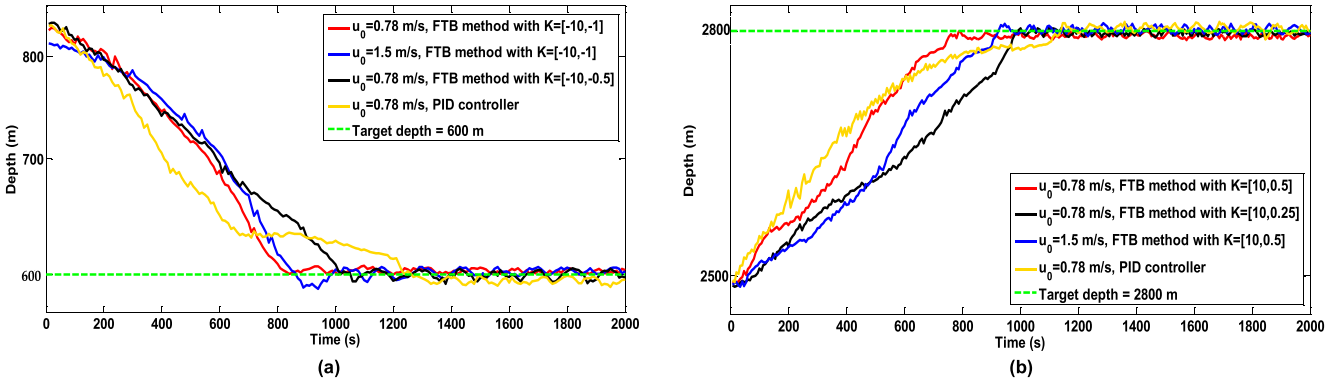

FIGURE 13. Depth experimental results for the closed-loop depth control system: (a) In ascending process, (b) In diving process.

Step 4: The measured depth value was recorded within the depth control time in the ascending or diving process. When the depth control time was reached, the depth control system operation was terminated.

Step 5: The DSIB was retrieved. The measured depth value and target depth were then compared. The transient time and depth error were obtained.

Step 6: According to the various cases and scenarios, the aforementioned experimental process was repeated by setting different control gains and different PID controller parameters or by deploying different current conditions.

The experiment results of the depth and the depth error from the sea trials are shown in Fig. 12 and Fig. 13, respectively. There are two scenarios used for testing the course of depth control. The experimental and simulation results illustrate the same trend in the depth error change. However, during the convergence process of the depth error, the fluctuations of the experimental results are more heavily damped than those of the simulation results. It is expected that the fluctuations can be caused by other uncertain factors besides the current disturbance, and the delay adjustment of the buoyancy-driven system. To evaluate the changes in the depth error during the steady state, the mean depth error was used. The comparison of the key experimental results in the ascending and diving processes is shown in Table 7. Compared with the simulation results, the DSIB took more time to converge to the desired depth, and had more depth error in the sea trial. In the ascending process, during the steady state, the depth error converged to a small neighborhood of 0 within 1300 s, and the mean depth error was less than 15 m. Whereas, in the diving process, during the steady state, the depth error converged to a small neighborhood of 0 within 2000 s, and the mean depth error was less than 15 m. Considering the maximum allowable error of depth positioning based on the actual hydrographic survey [30] and the depth control time of the depth control process, the above experimental results are considered practically acceptable. In Table 7, under the same current velocity of 0.78 m/s, in the ascending process, the transient time and depth error with the control gains $\boldsymbol{K} = [-10, -1]$ are 1078 s and 8.9 m, respectively. The same parameters with the control gains $\boldsymbol{K} = [-10, -0.5]$ are 1258 s and 11.2 m, respectively, In other words, the transient time and the depth error with the control gains $\boldsymbol{K} = [-10, -1]$ are less than those with $\boldsymbol{K} = [-10, -0.5]$. Similarly, under the same current velocity of 0.78 m/s in the diving process, the transient time and depth error with the control gains $\boldsymbol{K} = [10,0.5]$ are less than those with the control gains $\boldsymbol{K} = [10,0.25]$. In addition, in the ascending process, the transient time and depth error with PID controller are 1406 s and 15.6 m, respectively, which are larger than those with

TABLE 7. Comparison of key experimental results in ascending and diving processes.

Direction of motion	Experimental Scenario	Current velocity (m/s)	Controller parameters setup	Transient time (s)	Mean depth error (m)
Ascending process	Scenario 1 Case *a*	u_0=0.78	FTB method $\boldsymbol{K}$=[−10, −1]	1078	8.9
		u_0 = 1.5		1186	13.6
	Scenario 1 Case *b*	u_0=0.78	FTB method $\boldsymbol{K}$=[−10, −0.5]	1258	11.2
			PID controller k_p=5, k_i=0.5, k_d=20	1406	18.4
Diving process	Scenario 2 Case *a*	u_0=0.78	FTB method $\boldsymbol{K}$=[10, 0.5]	1369	9.8
		u_0 = 1.5		1472	14.2
	Scenario 2 Case *b*	u_0=0.78	FTB method $\boldsymbol{K}$=[10, 0.25]	1816	12.6
			PID controller k_p=5, k_i=0.2, k_d=30	1926	19.6

K = [−10, −0.5]. The same conclusion can be arrived at in the diving process as well. Furthermore, in the ascending process, the transient time and depth error with identical control gain under a current velocity of 1.5 m/s are 1186 s and 13.6 m, respectively, which are larger than those under a current velocity of 0.78 m/s. The same conclusion can be arrived at in the diving process as well. Thus, it can be inferred that compared to the PID controller under external disturbances, the depth positioning of the DSIB can be achieved by the FTB method with better accuracy and faster response in a finite time. Thus, the experiments have verified the effectiveness of the proposed depth controller. Thus, the experiments have verified the effectiveness of the proposed depth controller.

Furthermore, the adjustment rule of the control gains under the current disturbances in the simulations is verified by the experiment results. The results from the simulations and at-sea experiments are contrasted by using two different motion directions of the DSIB and target depth. The control gains are used to regulate the transient state of the state trajectories under the current disturbances. The performance of the depth positioning can be reflected by the depth error and the transient time. Under the same current disturbances, when the DSIB ascends with the control gains increasing or dives with the control gains decreasing, the transient time increases; the depth error grow larger; and the convergence rate of the state trajectories slow down. Similarly, with the identical control gains, when the DSIB ascends or dives with the current disturbances decreasing, the transient time decreases; the depth error grow smaller; the convergence rate of the state trajectories speeds up. In summary, the aforementioned analysis results provide an effective mechanism for adjusting the control gains under various current disturbances within a finite time.

VI. CONCLUSION

In this study, a buoyancy-driven DSIB was the object of research interest. Based on the pressure hull deformation of the DSIB, the dynamic model of the DSIB under ocean current disturbances was modeled. In order to realize depth control in a finite time, the method of OEIPP was introduced to establish the finite-time transformation matrix of the closed-loop depth control system. A FTB depth control strategy was proposed to solve the problem of transient stability under the cluttered current disturbances within a finite time. According to the measured data of the seawater density and current velocity in the South China Sea (15.5°N, 115.5°E and 14°N, 116°E), the performance of the proposed depth control strategy was assessed and verified through simulations and at-sea experiments. Results from the simulations and the at-sea experiments establish that the proposed FTB depth control method enables the DSIB to reach the allowable depth error of 15 m under current disturbances within 2000 s. Thus, the designed depth control strategy has been proved effective for the depth control process of the DSIB. Additionally, the smaller depth error and faster convergence are achieved by the FTB method in a finite time compared with the standard PID controller. The FTB method performs better control performance than the standard PID controller in the depth control process. Furthermore, for the hydrologic survey of a hovering depth from the sea surface to 4000 m underwater, the results based on FTB depth control method provide a guideline for adjusting the control gains of the depth control process under various current disturbances within a finite time.

ACKNOWLEDGMENT

The authors wish to thank the State Key Laboratory of Precision Measuring Technology and Instruments for their helpful comments.

REFERENCES

[1] R. E. Davis, L. A. Regier, and J. Dufour, "The autonomous Lagrangian circulation explorer (ALACE)," *J. Atmos. Ocean. Technol.*, vol. 9, no. 3, pp. 264–285, 1992.
[2] Eric A. D'Asaro, D. M. Farmer, J. T. Osse, and G. T. Dairiki, "A Lagrangian float," *J. Atmos. Ocean. Technol.*, vol. 13, no. 6, pp. 1230–1246, 1996.
[3] R. E. Davis, J. T. Sherman, and J. Dufour, "Profiling ALACEs and other advances in autonomous subsurface floats," *J. Atmos. Ocean. Technol.*, vol. 18, no. 6, pp. 982–993, 1999.
[4] K. Izawa, K. Mizuno, and M. Miyazaki, "On the weight adjustment of profiling floats," Japan Mar. Sci. Technol. Center, Yokosuka, Japan, ARGO Tech. Rep. FY2001, 2002, no. 5, pp. 18–35.
[5] E. A. D'Asaro, "Performance of autonomous Lagrangian floats," *J. Atmos. Ocean. Technol.*, vol. 20, no. 6, pp. 896–911, 2003.

[6] D. D. Swift and S. C. Riser, "RAFOS floats: Defining and targeting surfaces of neutral buoyancy," *J. Atmos. Ocean. Technol.*, vol. 11, no. 4, pp. 1079–1092, 2009.
[7] A. Schwithal and C. Roman, "Development of a new Lagrangian float for studying coastal marine ecosystems," in *Proc. IEEE Oceans*, May 2009, pp. 1–6.
[8] B. McGilvray and C. Roman, "Control system performance and efficiency for a mid-depth Lagrangian profiling float," in *Proc. IEEE Oceans*, May 2010, pp. 1–10.
[9] W. Jianguo, X. Huixi, and L. Jian, "Research on the buoyancy change of deep-sea autonomous underwater vehicle in the diving process," *Proc. ROBOT*, vol. 36, no. 4, pp. 455–460, 2014.
[10] R. N. Smith and V. T. Huynh, "Controlling buoyancy-driven profiling floats for applications in ocean observation," *IEEE J. Ocean. Eng.*, vol. 39, no. 3, pp. 571–586, Jul. 2014.
[11] V. Viswanathan and T. Taher, "Buoyancy driven autonomous profiling float for shallow waters," in *Proc. IEEE Oceans*, Sep. 2016, pp. 1–6.
[12] S. L. Reste, V. Dutreuil, X. André, V. Thierry, and C. Renaut, "'Deep-Arvor': A new profiling float to extend the argo observations down to 4000-m depth," *J. Atmos. Ocean. Technol.*, vol. 33, no. 5, pp. 1039–1055, 2016.
[13] L. Barker, "Closed-loop buoyancy control for a coastal profiling float," MBARI Intern Rep., Moss Landing, CA, USA, 2014, no. 8, pp. 1–15.
[14] J. Jouffroy, Q. Zhou, and O. Zielinski, "Towards selective tidal-stream transport for Lagrangian profilers," in *Proc. MTS/IEEE KONA*, Sep. 2011, pp. 1–6.
[15] R. N. Smith and V. T. Huynh, "Controlling buoyancy-driven profiling floats for applications in ocean observation," *IEEE J. Ocean. Eng.*, vol. 39, no. 3, pp. 571–586, 2014.
[16] K. P. Dahl, D. R. Thompson, D. McLaren, Y. Chao, and S. Chien, "Current-sensitive path planning for an underactuated free-floating ocean sensorweb," in *Proc. IEEE/RSJ Int. Conf. Intell. Robots Syst.*, Sep. 2011, pp. 3140–3146.
[17] P. Dorato, "Short time stability in linear time-varying systems," in *Proc. IRE Int. Conv. Rec. 4*, 1961, pp. 83–87.
[18] L. Weiss and E. F. Infante, "Finite time stability under perturbing forces and on product spaces," *IEEE Trans. Autom. Control*, vol. 12, no. 1, pp. 54–59, Feb. 1967.
[19] F. Amato, M. Ariola, and P. Dorato, "Finite-time control of linear systems subject to parametric uncertainties and disturbances," *Automatica*, vol. 37, no. 9, pp. 1459–1463, Sep. 2001.
[20] Z. Yan, H. Yu, W. Zhang, B. Li, and J. J. Zhou, "Globally finite-time stable tracking control of underactuated UUVs," *Ocean Eng.*, vol. 107, pp. 132–146, Oct. 2015.
[21] B. Sumantr, M. N. Karsiti, and H. Agustiawan, "Development of variable ballast mechanism for depth positioning of spherical URV," in *Proc. Int. Symp. Inf. Technol.*, Aug. 2008, pp. 1–6.
[22] A. Agrawal, B. Prasad, V. Viswanathan, and S. K. Panda, "Dynamic modeling of variable ballast tank for spherical underwater robot," in *Proc. IEEE Int. Conf. Ind. Technol. (ICIT)*, Feb. 2013, pp. 58–63.
[23] S.-P. Hsu and T.-S. Liu, "Modifications of control loop to improve the depth response of autonomous underwater vehicles," *Math. Problems Eng.*, vol. 2014, Aug. 2014, Art. no. 324813.
[24] Y. G. Sun, L. Wang, G. Xie, and M. Yu, "Improved overshoot estimation in pole placements and its application in observer-based stabilization for switched systems," *IEEE Trans. Autom. Control*, vol. 51, no. 12, pp. 1962–1966, Dec. 2006.
[25] Y. Wang, Y. Zou, Z. Zuo, and H. Li, "Finite-time stabilization of switched nonlinear systems with partial unstable modes," *Appl. Math. Comput.*, vol. 291, pp. 172–181, Dec. 2016.
[26] Y. Guo, S. Song, and L. Deng, "Finite-time coordination control for formation flying spacecraft," *J. Syst. Eng. Electron.*, vol. 25, no. 5, pp. 859–867, Oct. 2014.
[27] Y. Wang, Y. Liu, and Z. Zuo, "Finite-time boundedness of switched delay systems: The reciprocally convex approach," *IET Control Theory Appl.*, vol. 8, no. 15, pp. 1575–1580, 2014.
[28] Y. Wang, G. Wang, X. Shi, and Z. Zuo, "Finite-time stability analysis of impulsive switched discrete-time linear systems: The average dwell time approach," *Circuits Syst. Signal Process.*, vol. 31, no. 5, pp. 1877–1886, 2012.
[29] X. Lin, H. Du, S. Li, and Y. Zou, "Finite-time stability and finite-time weighted $l_2$2-gain analysis for switched systems with time-varying delay," *IET Control Theory Appl.*, vol. 7, no. 7, pp. 1058–1069, May 2013.
[30] J. I. Gobat and M. A. Grosenbaugh, "Time-domain numerical simulation of ocean cable structures," *Ocean Eng.*, vol. 33, no. 10, pp. 1373–1400, 2006.

ZURONG QIU received the Ph.D. degree in instrument and meter engineering from the School of Precision Instrument and Opto-Electronics Engineering, Tianjin University. He is currently a Teacher with Tianjin University. He is engaged in teaching and scientific research of precision mechanical design, ocean instrument design, ocean sensors, and so on. He has worked in Kingston University, U.K., and the Gintic Institute of Manufacturing Technology, Singapore, for international cooperation projects.

QIANG WANG received the M.S. degree in mechanical and electronic engineering from the Tianjin University of Technology, in 2013. He is currently pursuing the Ph.D. degree in instrument and meter engineering from the School of Precision Instrument and Opto-Electronics Engineering, Tianjin University. His current research interests include ocean observation and exploration technology, such as deep-sea intelligent float, wave power generation, and atmosphere duct measuring technology.

HONGYU LI received the Ph.D. degree in instrument and meter engineering from the School of Precision Instrument and Opto-Electronics Engineering, Tianjin University. He is currently a Teacher with the Shandong University of Science and Technology. He is also a part-time Teacher with the Qingdao Institute for Ocean Technology, Tianjin University. His current research interests include ocean observation and exploration technology, such as atmosphere duct measuring technology, deep-sea intelligent float, wave assessment.

SHAOBO YANG received the Ph.D. degree in instrument and meter engineering from the School of Precision Instrument and Opto-Electronics Engineering, Tianjin University. He is currently a Teacher with Tianjin University. His current research interests include ocean observation and exploration technology, such as atmosphere duct measuring technology, Argo float, and wave assessment.

XINGFEI LI received the Ph.D. degree in instrument and meter engineering from the School of Precision Instrument and Opto-Electronics Engineering, Tianjin University, where he is currently a Professor. His main research interests include ocean observation and exploration technology, such as ocean multi-sensor fusion technology and measurement technology.